Ultrasonics 97 (2019) 11–18

Contents lists available at ScienceDirect

Ultrasonics

journal homepage: www.elsevier.com/locate/ultras

A new radiation force balance method for measuring diverging piston source power in the frequency range 20–100 kHz: Theory and experimental verification

Wende Shou[a,*], Bing Hu[a], Lili Yu[b], Shimei Duan[c], Yi Chen[d], Yongjun Huang[d], Wei Zhang[a], Shuzhong Bu[e], Longyang Jia[a]

[a] Shanghai Institute of Ultrasound in Medicine, Shanghai Jiao Tong University Affiliated Sixth People's Hospital, China
[b] Shanghai Maritime University, China
[c] Center of Certification & Evaluation, Shanghai Food and Drug Administration, China
[d] Hangzhou Institute of Applied Acoustics, China
[e] Kunshan Risun Electronc Co. Ltd., China

ARTICLE INFO

Keywords:
Radiation force balance (RFB)
Semi-spherical target
Strongly diverged beam
Low ultrasonic frequency
Phase inverse mirror-image model

ABSTRACT

The purpose of this work was to present the results of a theoretical and experimental study in which a new acoustic output power measurement method was developed for a strongly diverged ultrasonic beam ($ka < 3$, where k is the circular wave number and a is the radius of transducer) using acoustic radiation force. To the best of our knowledge, there is no acceptable and effective method to measure acoustic power P for diverging piston transducers from 20 kHz to 100 kHz in the range $ka < 3$, it is a unsolved problem acutely. In the study, we used radiation force balance (RFB) method with a novel concave semi-spherical absorbing target in far field to measure the acoustic power up to 54 W. Based on the phase inverse mirror-image model we developed and Bridge's product theorem, the axial radiation force F on the target was first calculated and measured. The maximum difference of the ratio $r_{P/cF}$ ($=P/cF$) between theoretic and experimental values was smaller than 5%, where c is speed of sound in water. The reproducibility test of acoustic power measurements using two independent methods showed that the measurement uncertainty evaluated less than 10% by the new RFB method was much smaller than that (30%) by the traditional acoustic pressure method in underwater acoustics. It is indicated that the new RFB method is a primary and effective method for acoustic power measurement at least up to 20 W for frequency range 20 kHz to 100 kHz. The similar method was extended to power measurement for the rectangular transducer.

Based on this method a new primary method of hydrophone calibration was also developed.

1. Introduction

The purpose of this work was to establish the new acoustic power measurement method for highly diverging piston transducers based on RFB method in frequency range 20–100 kHz through theoretical study and experimental verification. The RFB as a primary method has been applied in ultrasonic power measurement for the non-focusing and the focusing beam and defined as an IEC standard method [1]. However up to now it has not yet been used for diverged beams whose radius of radiation surface is smaller than the wavelength, usually in low ultrasonic frequency such as $ka < 5$ for 20–100 kHz because all the measuring targets that have been used are incapable to intercept the entire power of full beams. Although a secondary measurement method was described for the value of derived (not true) acoustic output power of a ultrasonic surgical system in IEC 61847 [2,3], it is only feasible to use point sources such as the tips of surgical heads rather than general piston transducers.

The diverging transducers are used in ultrasonic cleaning, applications of sonochemistry and medicine etc. Using the mirror imaging principle, the acoustic field generated by a point acoustic source near an absolute soft boundary plane was described as a dipole by Skudrzyk E.[2,4], G Du et. al. [5] Based on this principle we first developed the phase inverse mirror-image model for the transducer immersed downward in water near the air-water interface Applying Bridge's product theorem [6] and Beissner's formulas [7] the ratio of the acoustic power (P) to the product of axial radiation force (F) and speed of sound (c), $r_{P/}$

* Corresponding author.
E-mail address: wdshou@163.com (W. Shou).

https://doi.org/10.1016/j.ultras.2019.03.019
Received 2 July 2018; Received in revised form 26 March 2019; Accepted 27 March 2019
Available online 03 April 2019
0041-624X/

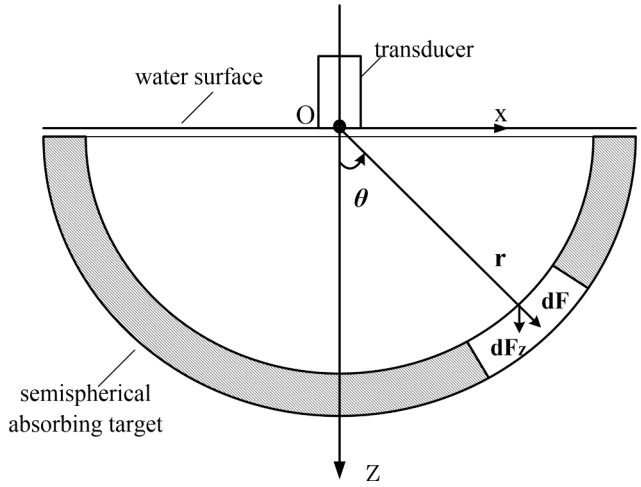

Fig. 1. The geometry of the circular plane transducer with water surface as a reflecting buffer and the concave semi-spherical absorbing target in the far field [7]

$_{cF}$, the directivity function $D(\theta)$, and the directivity index R_θ of the synthetic acoustic field of both the direct radiation from transducer and the reflection from the water surface were derived and verified via experiments. A RFB with a concave semi-spherical absorbing target in far field was set up to measure the acoustic power for circular transducers in 20–80 kHz [8]. A similar method can also be used to measure the acoustic power of the rectangular transducer.

A calibration method of the un-calibrated hydrophones used to measure the synthetic directivity pattern was developed.

2. Principle

The acoustic field in full space generated by a small ($ka < 5$) transducer downward under water is divergent. In our set-up, the backward wave component is reflected to the forward direction by the air-water interface. A large upward concave semi-spherical absorbing target in the far field encircling the down semi-space was designed for the RFB to intercept and capture total acoustic energy of the transducer right under the water surface downward as shown in Fig. 1 [7]. The total field is a superposition field of the direct and the reflected waves. The output power of the transducer P on the target surface can be calculated by the intensity integral shown in Eq. (1). The axial radiation force F on the target is also calculated by a similar integral of cosθ times of the intensity given in Eq. (2) [7].

$$P = \iint_S I dS \tag{1}$$

$$F = \frac{1}{c}\iint_S I\cos\theta dS \tag{2}$$

where I is the acoustic intensity as a function of the location in far field on the surface of the semi-spherical absorbing target with inner radius r and its origin is the center of the radiating surface, θ is the direction angle in $[0, \pi/2]$, S is the surface of target, $ds = r^2\sin\theta d\theta d\varphi$ is the element area in S, and φ is the azimuth or the polar angle of the field point's shadow in xy plane in $[0,2\pi]$, $r > \pi a^2/\lambda$ for the condition of the far field, λ is the wave length.

The ratio $r_{P/cF}$ is derived

$$r_{P/cF} = \frac{P}{cF} = \frac{\iint_S IdS}{\iint_S I\cos\theta dS} \tag{3}$$

where $I = I_0 D^2(\theta)$, $D(\theta)$is the normalized synthetic directivity function of the total field generated by the source transducer and by the

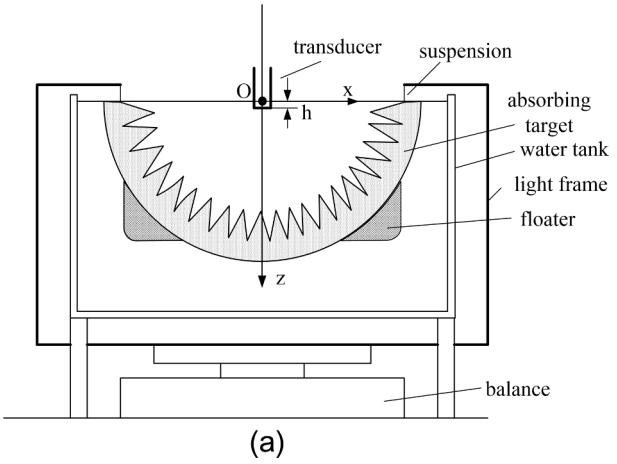

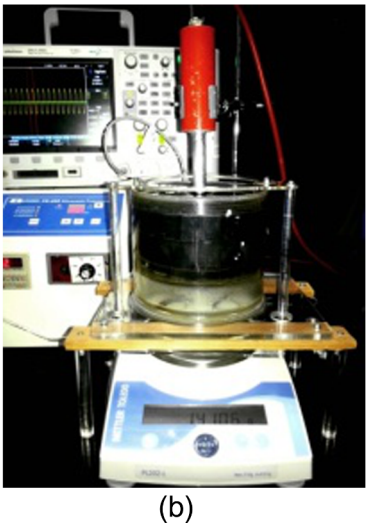

Fig. 2. The RFB with the semi-spherical absorbing target used to measure the acoustic power of a circular piston transducer in the frequency range 20 kHz-100 kHz [8] (a)schematic diagram (b) a photo of the experimental setup.

reflection of water surface, I_0 is the intensity at z = r on the beam axis z ($\theta = 0$). Since the azimuthal symmetry of the field, we have $\int_0^{2\pi} d\varphi = 2\pi$, then

$$r_{P/cF} = \frac{P}{cF} = \frac{\int_0^{\frac{\pi}{2}} D^2(\theta)\sin\theta d\theta}{\int_0^{\frac{\pi}{2}} D^2(\theta)\cos\theta\sin\theta d\theta} \tag{4}$$

Therefore, if the normalized synthetic directivity function is measured by using an un-calibrated hydrophone in the far field the ratio $r_{P/cF}$ can be calculated by the numerical method from Eq.(4). After determining axial radiation force F, we can calculate the acoustic power by using $P = r_{P/cF}\cdot cF$, if the attenuation of water is neglected. The schematic diagram of the RFB with a concave semi-spherical absorbing target is shown in Fig. 2 [8].

2.1. Theoretical model and calculation of $r_{P/cF}$ and R_θ

When a circular plane piston transducer with a downward beam axis is immersed in water near water surface, where immersion depth of the radiating surface is h, the acoustic field can be determined either by the phase inverse mirror-image model, or the dipole-piston field with the phase inversion mirror symmetry about the water surface, as the acoustic amplitude reflection coefficient of the water-air interface being −1 [4,5]. According to Bridge's product theorem the synthetic directivity function of this combined field of the transducer and its phase

reverse virtual image equals the product of the directivity function of the single piston transducer itself $Jinc(kasin\theta) = 2J_1(kasin\theta)/kasin\theta$ and that of a dipole of point source sin (kh cosθ)/sinkh [5,6] i.e

$$D(\theta) = \frac{2J_1(ka\sin\theta)}{ka\sin\theta}\cdot\frac{\sin(kh\cos\theta)}{\sin kh} \quad r > \pi a^2/\lambda,\ 20h \tag{5}$$

where $r > 20h$ is the approximate condition of the directivity function expression of dipole.

Substitute Eq. (5) into Eq. (4) to get Eq. (6)

$$r_{P/cF} = \frac{P}{cF} = \frac{\int_0^{\frac{\pi}{2}} [\frac{2J_1(ka\sin\theta)}{ka\sin\theta}\cdot\frac{\sin(kh\cos\theta)}{\sin kh}]^2 \sin\theta d\theta}{\int_0^{\frac{\pi}{2}} [\frac{2J_1(ka\sin\theta)}{ka\sin\theta}\cdot\frac{\sin(kh\cos\theta}{\sin kh}]^2 \cos\theta\sin\theta d\theta} \tag{6}$$

The values of $r_{P/cF}$ as the function of ka and kh are listed in Table B.1 of Appendix B. When ka and kh are given the corresponding $r_{P/cF}$ can be determined by the linear interpolation using the data listed in the table.

Substitute $I = I_0 D^2(\theta)$ into Eq. (1) and the directivity index R_θ, the crucial parameter for acoustic power measurement by the acoustic pressure method, can be expressed as Eq. (7) [6]

$$R_\theta = \frac{I_0}{(P/4\pi r^2)} = 2/\int_0^{\pi/2} D^2(\theta)\sin\theta d\theta \tag{7}$$

Substitute Eq. (5) into Eq. (7) to get Eq. (8)

$$R_\theta = 2\ /\ \int_0^{\frac{\pi}{2}} [\frac{2J_1(ka\sin\theta)}{ka\sin\theta}\cdot\frac{\sin(kh\cos\theta)}{\sin kh}]^2 \sin\theta d\theta \tag{8}$$

The parameters of $r_{P/cF}$ and R_θ vs. ka and kh were calculated using Eq. (6), Eq. (8) respectively. Their results for $kh << 1$ are shown in Fig. 3. For a point source $a \approx 0$, the model becomes a dipole and $P/(cF) = 1.333$ and $R\theta = 6$ where $kh \ll 1$.

Similarly, the ratio $r_{P/cF}$ can also be derived for a rectangular transducer with the ratio of length to width more than $\sqrt{2}$ mounted downward in water near surface. See Appendix A.

2.2. Experiment verification for calculation

Using the method described in IEC 61847:1998 [1] the synthetic directivity pattern of direct and reflection waves was measured for two transducers A and B.

An anechoic tank used of 2 m in length, 1 m in width, and 1.5 m in depth was stuck with rubber wedge absorbers on all the walls. The experimental setup of measuring the synthetic directivity pattern of transducer field is shown in Fig. 4. The transducer's radiation surface was fixed downward at the immersion depth h of 2 mm. The experiment was completed in the Lab of Hangzhou Institute of Applied Acoustics in China. The measuring hydrophone B & K 8103 was placed at the position with a distance R at the beam axis z from water surface where $R > 20h$ and $\pi a^2/\lambda$.

The hydrophone fixed at a movable J-shaped stand in the tank was scanning with 20 angle steps in the xz plane and yz plane respectively along the semicircular arches of radius $R = 129$ mm with the same center at the point O, where the transducer symmetric axis and the water surface intersected. The data of synthetic directivity pattern were measured for two transducers of A (20.08 kHz, $a = 7.5$ mm) and B (85.24 kHz, $a = 6.5$ mm). Their synthetic directivity patterns determined are shown in Fig. 5.

The average values of the measured beam widths in two scan planes, the measured R_θ and $r_{P/cF}$ and their theoretically calculated value for transducer A and B are listed in Table 1.

For transducers A and B, the maximum relative difference between the average measured value and the theoretical calculated value is less than 7.6% for R_θ and 4.5% for $r_{P/cF}$ respectively, indicating a good consistancy.

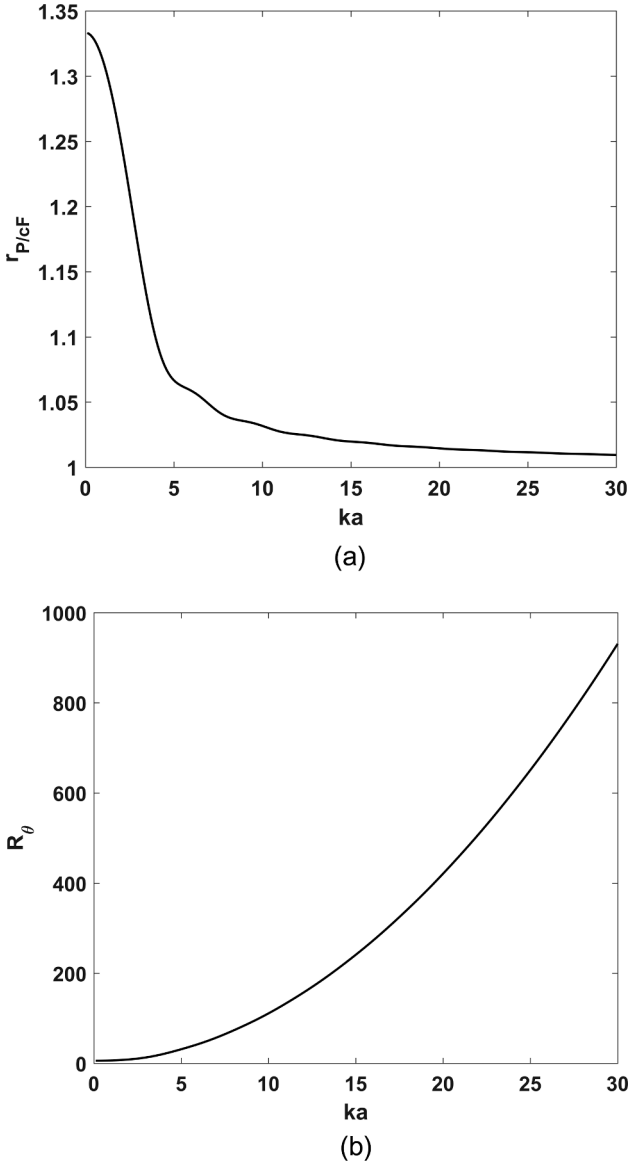

Fig. 3. The curves of $r_{P/cF}$ (a) and R_θ (b) vs. ka where $kh << 1$.

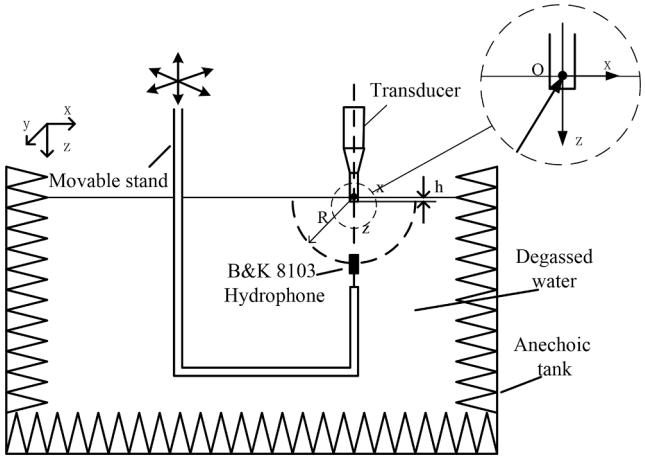

Fig. 4. The measurement system of synthetic directivity pattern of the field generated by a transducer immersed in water and near water–air interface surface.

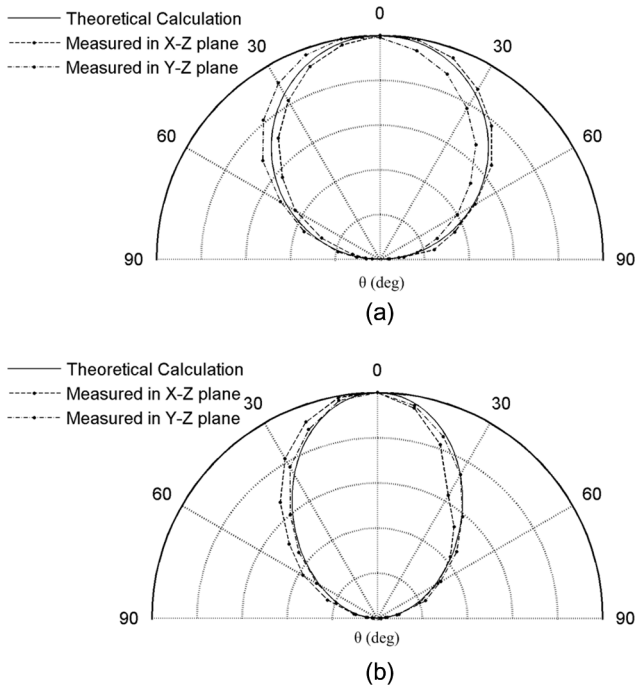

Fig. 5. The synthetic directivity patterns measured compared with that calculated theoretically for transducers A (a) and B (b).

Table 1
The average values of the beam widths, R_θ and $r_{P/cF}$ measured and theoretically calculated values for transducers A and B.

Transducer	Parameter	$\theta_{.3dB}$	$\theta_{.6dB}$	$\theta_{.10dB}$	R_θ	$r_{P/cF} = P/cF$
A (20.08 kHz,	Y_T	88.00°	117.00°	141.40°	6.28	1.32
a = 7.5 mm,	Y_E	85.20°	114.10°	140.30°	6.34	1.33
ka = 0.652,	Δ (%)	3.18	2.48	0.78	1.05	0.45
kh = 0.174)						
B (85.24 kHz,	Y_T	64.00°	90.00°	116.00°	9.71	1.23
a = 6.3 mm,	Y_E	64.60°	93.65°	122.20°	8.98	1.17
ka = 2.40,	Δ (%)	0.94	4.06	5.17	**7.59**	4.48
kh = 0.738)						

Note: Y_T is the theoretically calculated value using the radius of radiation surface a and formulas (5), (6), (8).
Y_E is the measured value using the experimental data of directivity pattern and formulas (4), (7).
$\Delta = |Y_E - Y_T|/Y_T$ is the relative difference. h = 2 mm.

3. Reproducibility test of acoustic power measurement

Our theoretical and experimental studies demonstrate that the acoustic output power of the circular transducer immersed in water near water surface can be determined well by RFB. Traditionally, it can also be measured by a calibrated hydrophone. To test the credibility of the RFB method the radiation conductance parameters of two transducers A, and C were also calculated theoreticaly and measured experimentally for coparison of values $r_{P/cF}$ and R_θ in the two methods.

3.1. Acoustic power measurement by RFB

The semi-spherical absorbing target with outside diameter 100 mm of the RFB shown in Fig. 2 was made of SA-J35 sulfur removal rubber wedge absorber (Hangzhou Institute of Applied Acoustics, Hangzhou, China). Its sound (power) absorption coefficient, defined as the sum of the sound (power) dissipation coefficient and the sound (power) transmission coefficient for the sound energy flux, was greater than 99% and the echo reduction greater than 20 dB in frequency range 20 kHz to 200 kHz. The degassed water with the oxygen concentration less than 3 ppm was used. The immersion depth of aperture plane of target in water was less 2 mm. The immersion depth of radiating surface h was 2 mm.

The experiment was completed in the Shanghai Acoustic laboratory of Chinese Academy of Sciences. A multiple function generator NF1974 (NF corporation, Japan) and a Precision Power Analyzer PPA 2500 (Kineti Q) were used to produce output and detect the exciting voltage of the transducer $U_{Trms,}$. The axial radiation force acting on the target F was measured by the balance (SE 2020, OHAUS Corp., USA). Then the output power P is given in the following

$$P = r_{P/cF} cF(1 + \gamma^2)^{-1} e^{2\alpha r} \tag{9}$$

where γ is the amplitude reflection coefficient of the target, $\gamma = 0.1$; α is the attenuation coefficient of water; $r = R$ is the inner radius of the semi-spherical target, R = 40mm.

The radiation conductance of a transducer G is equal to the output power P divided by the square of exciting root mean square voltage U^2_{Trms}, i.e.

$$G = P/U^2_{\mathrm{Trms}}. \tag{10}$$

The results of transducer A and D are shown in Tables 2 and 3 and Fig. 6.

The measured G of transducer C (80.3 kHz, Ø 13 mm) is 1.72mS by RFB. See Table 5.

The average value G_{av} of the radiation conductance of transducer A and D is 3.88 mS and 2.69 mS respectively, and their corresponding value G_d of dynamic radiation conductance, i.e. the slop of fitting lines in Fig. 6, is 4 mS and 2.44 mS.

3.2. Acoustic power measurement by acoustic pressure method using calibrated hydrophone

Based on the definition of directivity index in Eq. (7) the output power of a circular piston transducer under our experimental condition can be expressed [6,9] as following

$$P = \frac{2\pi l^2}{\rho c R_\theta}\left(\frac{U_H}{M_L}\right)^2 e^{2\alpha l}.\ l > 20\ \ h, \quad \pi a^2/\lambda \tag{11}$$

where l is the distance between the hydrophone's center at the beam axis and water surface; ρ is the water density, U_H is the measured output voltage of hydrophone, M_L is free field cable-ended voltage sensitivity of the hydrophone, α is the attenuation coefficient of water.

In the directivity pattern measurement using the calibrated hydrophone B & K8103 the power P can be given as R_θ, l, U_H, α and M_L were known.

The measurement results of radiation conductance by RFB and by the acoustic pressure method for two transducers A and C are listed in Tables 4 and 5. In these tables, the subscripts P and R of G denote value measured G by acoustic pressure method and by RFB respectively.

It can be seen from Tables 1 and 5 that the maximum relative difference of $r_{P/cF}$ between the experimental and theoretical values is 4.5%, and that of R_θ is 11.4% for transducers A, B, C.

The results by RFB were compared with that by the traditional acoustic pressure method using R_θ for transducers A and C. The maximum relative difference of G between by the acoustic pressure method (use R_θ) and by RFB (use $r_{P/cF}$) using experimental values is 4.6%. If

Table 2
The output power and radiation conductance of transducer A (20.08 kHz, a = 7.5 mm) measured by RFB.

U_{Trms} (V)	20.11	25.24	30.14	35.13	40.21	45.00
P (W)	1.64	2.31	3.47	4.82	6.27	8.10
G (mS)	4.04	3.63	3.82	3.90	3.88	4.00

Table 3
The measured result of another transducer D (40.22 kHz, a = 1.77 mm) by RFB.

U_{Trms}(V)	31.9	65.8	99.0	116.0	136.6	147.5
P(W)	1.19	11.5	25.1	39.5	52.4	54.4
G(mS)	1.17	2.65	2.56	2.93	2.84	2.50

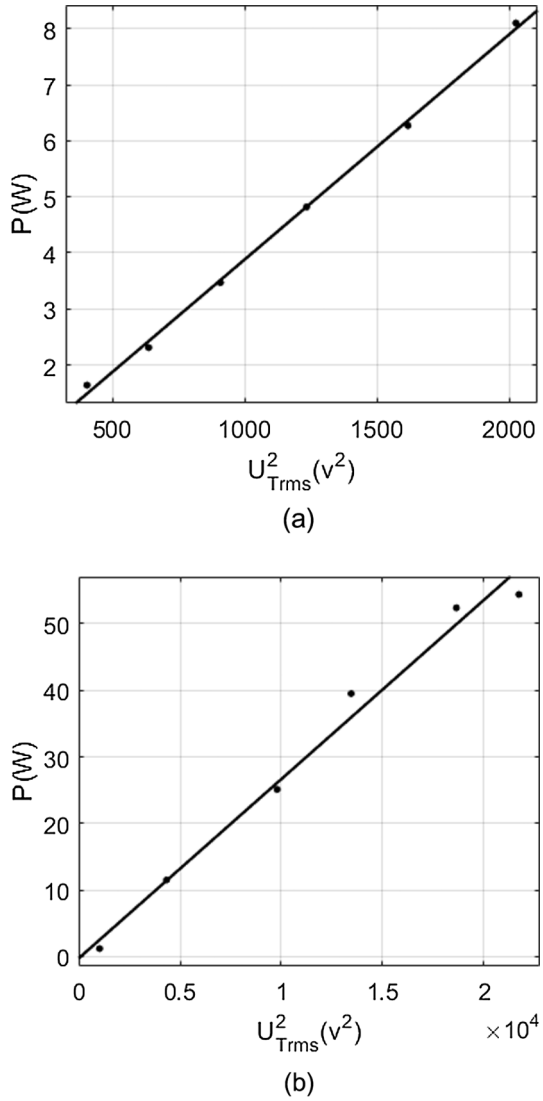

Fig. 6. The fitting line of output power P vs. exciting voltage squared$U^2_{Trms}$of transducers A (a) and D (b) by RFB.

Table 4
The average theoretical and measurement results of transducer A (20.08 kHz, Ø15 mm) by RFB and acoustic pressure methods.

Method	Parameter	Theoretic Result Y_T	Experiment Result Y_E	$\lvert\Delta Y_{E-T}/Y_T\rvert$ (%)
Acoustic pressure method (l = 190 mm)	R_θ	6.28	6.34	1.05
	G_P(mS)	3.74	3.70	1.07
RFB (r = 15 mm)	$r_{P/cF}$	1.32	1.33	0.45
	G_R (mS)	3.86	3.88	0.52
$\Delta G_{P\text{-}R}/G_R$ (%)	$(G_P - G_R)/G_R$	−3.11	−4.64	

Note: The free field cable-end loaded sensitivity of hydrophone B&K8103 used is 2.82 × 10–5 V/Pa (−211.0 dB re 1 V/μPa at 20 kHz); The attenuation of water is negligible for distances of 190 mm at 20.08 kHz.

Table 5
The average theoretical and measurement results of transducer C (80.3 kHz, Ø 13 mm) by RFB and acoustic pressure methods.

Method	Parameter	Theoretic result Y_T	Experiment result Y_E	$\left\lvert\frac{\Delta Y_{E-T}}{Y_T}\right\rvert$(%)
acoustic pressure method (l = 157 mm)	R_θ	9.17	10.47	11.40
	G_p(mS)	1.92	1.68	12.00
RFB (r = 15 mm)	$r_{P/cF}$	1.24	1.24	0.41
	G_R (mS)	1.71	1.72	0.59
$\Delta G_{P\text{-}R}/G_R$ (%)	$(G_P - G_R)/G_R$	11.20	−2.62	

Note: The free field cable-end loaded sensitivity of hydrophone B&K8103 used is 2.66 × 10–5 V/Pa (−211.5dBre 1 V/μPa at 80 kHz); The attenuation of water is negligible for distances of 157 mm at 80.3 kHz.

using their theoretical values that is 11.2% which is caused by the great difference of the R_θ values 11.4% between the theory and the experiment. So the maximum relative difference of G between usages of the experimental and theoretical values of $r_{P/cF}$ is 0.59% in RFB method, and that of R_θ is 12.0% in the acoustic pressure method.

4. Hydrophone calibration

After measuring $r_{P/cF}$ and R_θ by an un-calibrated hydrophone and G by RFB the sensitivity M_L of the used hydrophone can be calibrated based on the constant radiation conductance for the transducer in linear range. Then combining Eqs. (9)–(11), the following formula can be given

$$M_L = \frac{2\sqrt{\pi}lU_{Hrms}U_{TRFB}(1+\gamma^2)^{1/2}}{U_{TR_\theta}c(R_\theta\rho r_{P/cF}F)^{1/2}}e^{\alpha(l-r)} \tag{12}$$

where U_{TRFB} is the exciting voltage of the transducer in RFB method; $U_{TR_\theta}$is that inthe directivity pattern measurement; U_{Hrms} is the output RMS voltage of the hydrophone at the position z = l on the beam axis in far field. L = 190 mm, r = 65 mm.

The calibrated free field cable-end loaded voltage sensitivity of the used B & K 8103 hydrophone M_L at 20.08 kMz is 2.75 × 10–5 V/Pa (−211.1 dB re 1 V/μPa) using transducer A, very close to its normal value −211.9 dB. The specific load terminating B &K 8103 hydrophone is 10 MΩ and 11 pF.

5. Conclusion and discussion

In low ultrasonic frequency range from 20 kHz to 80 kHz, the wavelength is greater than the dimension of transducers so that their Rayleigh's length (distance) $\pi a^2/\lambda$ is only several millimeters e.g. if a = 7.5 mm, $\pi a^2/\lambda$ = 2.36 mm for 20 kHz and 9.4 mm for 80 kHz, and the acoustic field is diverged. The field characteristics of these transducers downward under and near water surface can be expressed by the synthetic directivity function of the direct wave from the transducer and the reflection wave from the water surface.

For any new RFB system the primary key issue is to define the correct method determing the parameter$r_{P/cF}$ of the combination of the system and the transducer to be measured in both theory and experiment since$r_{P/cF}$ is the most important factor of measurement accuracy for acoustic power.

In the study, the phase reversed mirror-image model (dipole-piston model) was used to analyze the acoustic field. Accordingly, the synthetic directivity function was derived based on Bridge's product theorem and also measured in experiments. The ratio $r_{P/cF}$ and the synthetic directivity index R_θ were calculated using the theoretic and experimental data.

The $r_{P/cF}$ is expressed the quotient whose cumulative function of divisor is cosθ times of the cumulative function of dividend. The divisor

and dividend have some similarity especially for small θ so that the change of directivity pattern effects the quotient $r_{P/cF}$ weakly but R_θ obviously. In theory, when $kh \ll 1$ the relative change of $r_{P/cF}$ for transducer in the ka ranged from 0 to 5 is -20% only, but that of R_θ is 425% as shown in Fig. 3. The maximum relative difference of $r_{P/cF}$ between the experimental and theoretical values is smaller than 4.5% for transducers A,B,C and 2.5 times less than 11.4% of R_θ.

In reproducibility tests of the two methods for transducers A and C the measured values G by these two methods are close (the maximum difference $\Delta_{max} < 4.64\%$) if only use the experimental values of R_θ or $r_{P/cF}$. It also close to that by RFB using the theoretical values of $r_{P/cF}$ (Δ_{max}<5.1%). These results indicate that the theoretical calculated values of $r_{P/cF}$ could be directly used in power measurement for the transducer of $ka < 5$. It simplifies the measurement procedure greatly. The acoustic power measurement by RFB is of better accuracy than that by the acoustic pressure method. The RFB is an absolute or primary method with measurement uncertainty much better than 10%, but the acoustic pressure method is a secondary method with measurement uncertainty 30%, including the uncertainty of hydrophone calibration 10% generally [8]. In our study the good consistancies of $r_{P/cF}$ and G in threory and experiment were reached.

The upper limit of acoustic power measurement by RFB method is dependent on the cavitation on the radiating surface of transducer especially when the tap water is used. The uses of good degassed water and minimized measurement time can effectively increase the upper limit. The nonlinear effect and the cavitation were not observed obviously in our measurement range when the oxygen concentration in water was less than 3 ppm and the radiating time was less than 20 s. The nonlinear effect could not influence the axial radiation force on the target.

Because the harmonic components have the directivity patterns sharper than that of the base wave component it can strengthen the axial radiation force. Acaustic streaming may also shtrenthen force on the target. As a result, they may compensate the loss increase of harmonic attenuation.

The fluctuation of water surface limited the maximum measurement power in experiments. The measured acoustic power is up to 54.4 W (552 W/cm^2) at 40.2 kHz where the estimated maximum streaming velocity at the center of the target surface is less than 8 mm/s according to the studies of J Kolb and W L Nyborg, and Y G Stanikov [10]. The maximum measured acoustic power at 20 kHz is up to 22 W now.

Experiments demonstrate that the new RFB method reported here is feasible and effective for measuring the output power of transducers of $ka < 5$ in frequency range 20 kHz to 100 kHz.

A new calibration method of the hydrophone was simultaneously established based on the RFB method when the hydrophone to be calibrated was needed to measure the directivity pattern.

These methods could also be applied to the acoustic power measurement and the hydrophone calibration in underwater acoustic frequency.

Acknowledgement

Authors are grateful to Ms. Lin Yanduan for her excellent work in abundant experiment.

Appendix A

Acoustic power measurement of rectangular transducer by RFB in low ultrasonic frequency

A.1. Ratio $r_{P/cF}$ of rectangular transducer with the ratio of length to width more than $\sqrt{2}$

When a rectangular transducer with short side 2a and long side L ($L \geq 2\sqrt{2}a$) is placed downward under and near water surface, the immersion depth of radiating surface is h. In the cylindrical coordinate system (r,θ,z), r is the radial distance, θ is the azimuth angle, height axis z is the intersected line of the water surface and the plane which both long sides are symmetrical about. R is the inner radius of a concave semi-cylindrical absorbing target whose central axis is axis z as shown in Fig. A.1(a), where $L^2/\pi\lambda > R > 4a^2/\pi\lambda$, $kh << 1$, $-L/2 < z < L/2$, λ is the wavelength. k is the circular wave number.

The acoustic power is [7].

$$P = \int_A IdA = \int_A I_0 D^2(\theta) dA = 2RLI_0 \int_0^{\pi/2} D^2(\theta) d\theta \tag{A.1}$$

Where $I = I_0 D^2(\theta)$, $D(\theta)$is the synthetic directivity function of the transducer and water surface. I_0 is the intensity at $\theta = 0°$, $r = R$. $A = \pi RL$ is the inner surface area of the semi-cylindrical target. d$A = RLd\theta$. The attenuation of water is neglected.

The axial radiation force is [7]

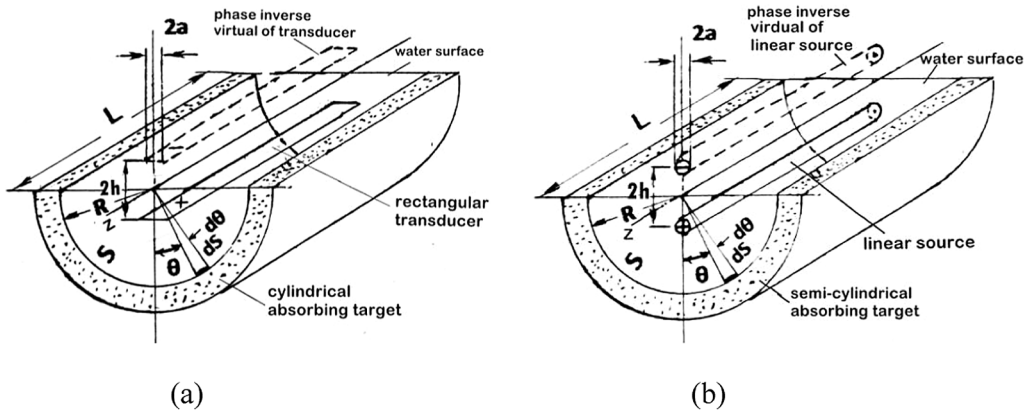

Fig. A.1. The schematic diagrams of the phase inverse mirror-image model for rectangular transducer (a) and for linear source (b) under and near water surface.

$$F = \frac{1}{c}\int_A I\cos\theta dA = \frac{2RLI_0}{c}\int_0^{\pi/2} D^2(\theta)\cos\theta d\theta \tag{A.2}$$

The ratio $r_{P/cF}$ is derived

$$r_{P/cF} = \frac{P}{cF} = \frac{\int_0^{\pi/2} D^2(\theta)d\theta}{\int_0^{\pi/2} D^2(\theta)\cos\theta d\theta} \tag{A.3}$$

The directivity function of the rectangular transducer is

$$D(\theta, \varphi) = \frac{\sin(ka\sin\theta)}{ka\sin\theta}\cdot\frac{\sin\left(\frac{kL}{2}\sin\varphi\right)}{\frac{kL}{2}\sin\varphi} \tag{A.4}$$

where φ is the elevation angle in plane z-r· When $r = R<L^2/\pi\lambda$ the beam in plane z-r is an un-divergent beam in the near field. For the viewpoint of geometric acoustics the pressure along each line parallel to axis z on effective inner surface of the target in the distance range -L/2 to L/2 is approximate constant respectively i.e. $\varphi = 0$ or $\sin(\frac{kL}{2}\sin\varphi)/(\frac{kL}{2}\sin\varphi) = 1$. Based on the phase inverse mirror-image model supposed using Bridge's product theorem, the synthetic directivity function of the transducer with the reflecting water surface in the azimuth planes where -L/2 < z < L/2 is given by the product of the directivity function of a rectangular transducer of width $2a$ itself, $\sin(ka\sin\theta)/ka\sin\theta$ and that of a dipole of polar distance $2h$,$\sin(kh\cos\theta)/\sin kh$ as following as

$$D_{(\theta)} = \frac{\sin(ka\sin\theta)}{ka\sin\theta}\cdot\frac{\sin(kh\cos\theta)}{\sin kh} \quad L^2/\pi\lambda > R > 4a^2/\pi\lambda, \quad 20h \tag{A.5}$$

where $R > 4a^2/\pi\lambda$, $20h$ is the condition for far field and for the approximate expression of directivity function of dipole respectively. $L^2/\pi\lambda > R$ is for $\varphi = 0$.

Substitute Eq. (A.5) into Eq. (A.3) to get Eq. (A.6)

$$r_{P/cF} = \frac{\int_0^{\pi/2} D^2(\theta)d\theta}{\int_0^{\pi/2} D^2(\theta)\cos\theta d\theta} = \frac{\int_0^{\frac{\pi}{2}} [\frac{\sin(ka\sin\theta)}{ka\sin\theta}\cdot\sin(kh\cos\theta)]^2 d\theta}{\int_0^{\frac{\pi}{2}} [\frac{\sin(ka\sin\theta)}{ka\sin\theta}\cdot\sin(kh\cos\theta)]^2\cos\theta d\theta} \tag{A.6}$$

For a linear source, see Fig. A.1(b), ka ≈ 0 and $kh \ll 1$,$r_{P/cF} = 1.18$.

A.2 The RFB to measure the acoustic output power of ultrasonic knife

The ultrasonic knife has a very small aperture $2a(\approx 0)$ and very long length L ($\gg \sqrt{\pi\lambda R}$)so that it is a typical linear source. When the knife is placed under and near water surface to be measured by the long concave absorbing target with the length more than $1.2L$ the ratio $r_{P/cF}$ is equal to 1.18.

A RFB was designed to measure the acoustic output power of three ultrasonic knifes with 82 mm, 120 mm and 190 mm of edge length operating in 40 kHz (Shanghai Jiaocheng Mechano- elctronic Equipment Co. Ltd., China) using a long absorbing target with V-shaved cross section as shown in Fig. A2. The values of measured acoustic output power of these knifes are 41.7 W, 37 W, 48.7 W in turn.

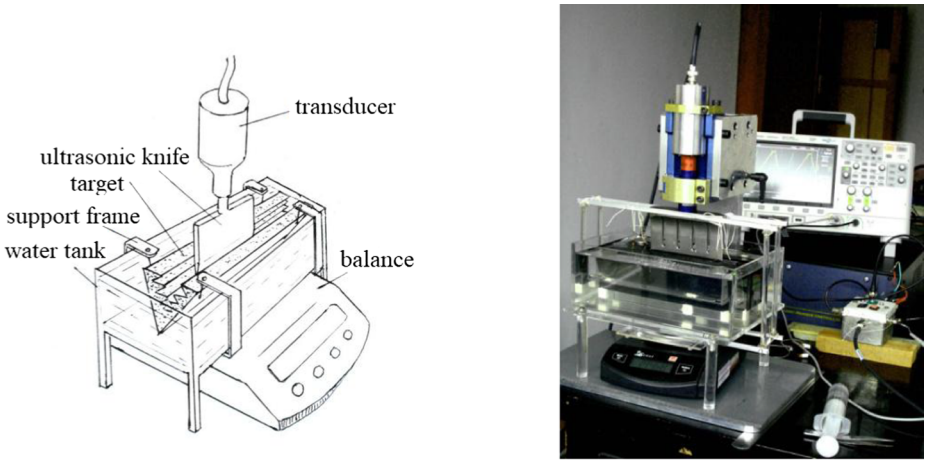

Fig. A.2. The RFB with a long absorbing target with V-shaped cross section for measuring the acoustic power of an ultrasonic knife operating in 40 kHz (a) schematic diagram and (b) photo of the experimental setup.

Appendix B

Values of $r_{P/cF}$ as function of ka and kh for circular piston transducers under water and near surface downward was listed in Table B.1.

Table B.1
The ratio $r_{P/cF}$ as the function of ka and kh ($R > 20h$, $\pi a^2/\lambda$).

	kh															
ka	0.15	0.20	0.25	0.30	0.35	0.40	0.45	0.50	0.55	0.60	0.65	0.70	0.75	0.80	0.85	0.90
0	1.334	1.335	1.335	1.336	1.337	1.338	1.339	1.341	1.343	1.344	1.346	1.348	1.351	1.353	1.356	1.359
0.25	1.333	1.333	1.334	1.335	1.336	1.337	1.338	1.339	1.341	1.343	1.345	1.347	1.349	1.352	1.355	1.357
0.50	1.328	1.329	1.33	1.33	1.331	1.333	1.334	1.335	1.337	1.339	1.341	1.343	1.345	1.347	1.35	1.353
0.75	1.322	1.322	1.323	1.324	1.324	1.326	1.327	1.328	1.33	1.332	1.333	1.335	1.338	1.34	1.343	1.346
1.0	1.312	1.313	1.313	1.314	1.315	1.316	1.317	1.318	1.32	1.322	1.324	1.326	1.328	1.33	1.333	1.335
1.25	1.3	1.3	1.301	1.302	1.303	1.304	1.305	1.306	1.308	1.309	1.311	1.313	1.315	1.317	1.32	1.322
1.5	1.286	1.286	1.287	1.287	1.288	1.289	1.29	1.291	1.293	1.294	1.296	1.298	1.3	1.302	1.304	1.307
1.75	1.269	1.269	1.27	1.271	1.271	1.272	1.273	1.275	1.276	1.277	1.279	1.281	1.282	1.284	1.287	1.289
2.0	1.251	1.251	1.252	1.252	1.253	1.254	1.255	1.256	1.257	1.258	1.26	1.261	1.263	1.265	1.267	1.269
2.25	1.231	1.231	1.232	1.232	1.233	1.234	1.234	1.235	1.236	1.238	1.239	1.24	1.242	1.244	1.245	1.247
2.50	1.21	1.21	1.211	1.211	1.212	1.212	1.213	1.214	1.215	1.216	1.217	1.218	1.22	1.221	1.223	1.225
2.75	1.189	1.189	1.189	1.19	1.19	1.191	1.191	1.192	1.193	1.194	1.195	1.196	1.197	1.198	1.2	1.201
3.0	1.167	1.168	1.168	1.168	1.169	1.169	1.17	1.17	1.171	1.172	1.173	1.174	1.175	1.176	1.177	1.178
3.5	1.128	1.129	1.129	1.129	1.129	1.129	1.13	1.13	1.131	1.131	1.132	1.132	1.133	1.134	1.134	1.135
4.0	1.097	1.097	1.098	1.098	1.098	1.098	1.098	1.098	1.099	1.099	1.099	1.1	1.1	1.1	1.101	1.101
2.5	1.077	1.077	1.077	1.077	1.078	1.078	1.078	1.078	1.078	1.078	1.079	1.079	1.079	1.079	1.08	1.08
5.0	1.067	1.067	1.067	1.067	1.067	1.067	1.067	1.068	1.068	1.068	1.068	1.068	1.069	1.069	1.069	1.07

References

[1] IEC61161 Ed.3: 2013 Ultrasonics - Power Measurement - Radiation force balances and performance requirements, Annex E, Fig. 1 and Fig.2, pp.38-41.
[2] IEC61847:1998, Ultrasonics-surgical systems-Measurement and declaration of the basic output characteristics , International Electrotechnical Commission, 1998.
[3] SCHAFER, M.E., BROADWIN, A. Acoustical Characterization of Ultrasonic Surgical Devices, 1994, IEEE Ultrasonics Symposium, pp.1903-1906.
[4] E. Skudrzyk, The foundations of acoustics, Springer Verlag, Vienna, 1971, p. 355.
[5] G. Du, Z. Zhu, X. Gong, Fundamental of Acoustics (in Chinese), Nanjing University Press, 2001 pp. 319–324, 331–332.
[6] Robert J. Bobber, Underwater Electroacoustic Measurements, Naval Research Laboratory, Washington, D C, July 1970, Chapter 2, pp. 73-90.
[7] K. Beissner, Radiation force calculation, Acta Acustica United with Acustica. 62 (62) (1987) 255–263.
[8] Chinese Patent: No.ZL201621461180.4, 2017. A radiation force balance for ultrasound in low ultrasonic frequency (in Chinese).
[9] GB/T 7965-2002: Acoustic-Underwater transducer measurements (in Chinese), National Standard of China, sub-clause 17.1.
[10] L D Rozenberg, translated from Russian by J S Wood, High intensity ultrasonic fields, Plenum Press,1970, Part III, pp.195-196.